Proceedings of the
Annual Stability Conference
Structural Stability Research Council
San Antonio, Texas, March 19-22, 2024

Design guidelines for enhanced stability of steel systems

Ali Imanpour[1]

Abstract
This paper presents the findings from full-scale experimental testing and advanced numerical simulations that led to the improvement of the stability design of four systems used in the construction of steel structures, including I-shaped welded steel girders, overhanging steel beams, steel concentrically braced frames, and steel moment-resisting frames. For each system, the stability response under anticipated loads, gravity, wind, seismic or the combination of these loads, are first described. The experimental test program and finite element simulation layout developed to examine the stability response of these systems are then presented followed by the results of physical testing and numerical simulations used to propose stability design recommendations or verify the available design methods for these steel systems. The challenges of designing experimental programs or developing numerical models for stability response evaluation are also discussed for each studied system followed by the techniques developed to overcome these challenges.

1. Introduction

The stability of steel structures has been studied for decades with the aim of enhancing our understanding of structural behavior and developing improved structural design methods that can better represent the response of steel structures to applied loads. Recent decades have witnessed remarkable progress in structural testing equipment, facilities, computational power and numerical simulation tools to evaluate complex structural problems under various loading and boundary conditions anticipated in real structures. Nowadays, full-scale testing and high-fidelity numerical simulation of structural systems, subassemblies and connections have become routine. These advanced tools paved the way for a deeper understanding of complex structural stability problems, ultimately leading to the development of enhanced stability design guidelines for steel systems under various loads, such as gravity, wind and earthquake.

This paper presents the findings from full-scale experimental testing and advanced numerical simulations that led to improvement of the stability response of and development of design provisions for four steel systems, including 1) I-shaped welded steel girders, often used in the construction of steel buildings and girder bridges, that are subjected to vertical gravity loads, 2) overhanging steel beams, typically used as the roof framing system of single-story steel buildings in North America, under gravity- and wind-induced vertical loads, 3) steel concentrically braced

[1]Associate Professor, University of Alberta, <imanpour@ualberta.ca>

frames (CBFs), employed as the seismic force-resisting system of building structures, under gravity plus seismic loads and 4) wide-flange columns of steel moment-resisting frames (MRFs), used in the construction of low- to mid-rise steel buildings in high seismic regions, subjected to gravity plus seismic loads. For each system, a background and rationale for research is presented, followed by the research objectives and details of the experimental test procedure or numerical model layout. Challenges encountered, when designing the test program or developing numerical models, and their corresponding solutions are also described for each of these systems. Finally, the results of the response evaluation and the proposed design recommendations are presented and discussed.

2. I-shaped Welded Steel Girders

2.1 Background

I-shaped welded steel girders are often used in the construction of steel buildings and girder bridges. To select an appropriate cross-section at ultimate limit states, their flexural and shear resistances shall be verified. The limit states associated with the flexural resistance include cross-sectional yielding, lateral–torsional buckling (LTB), and local buckling. When relatively slender webs ($h/w > 90$ where h and w are the depth and thickness of the web, respectively) with torsionally-stiff flanges are used to construct these girders, the lateral–distortional buckling (LDB) limit state may also control the flexural response of the member. LDB involves displacement of the web-flange intersection in combination with web bending and cross-sectional twist, which results in distortion in the web, thus reducing the effective St. Venant torsional stiffness of the section and leading to a reduction in the flexural strength (White and Jung 2007). The LDB mode has not been explicitly considered by the North American steel and bridge design standards, including the Canadian steel design standard CSA S16-19 (CSA 2019a), Canadian highway bridge design standard CSA S6-19 (CSA 2019b), AISC Specification for Structural Steel Buildings (AISC 2022), and AASHTO LRFD Bridge Design Specifications (AASHTO 2020). Furthermore, North American steel building and bridge design standards do not differentiate between the flexural capacity of hot-rolled and welded I-shaped girders, despite the potential influence of the fabrication procedure, e.g., plate cutting method in welded girders, and material on the flexural capacity of welded girders (Bjorhovde et al. 1972; Chernenko and Kennedy 1991). In contrast, Eurocode 3, EC3 (EN1993-1-1 2005) differentiates the flexural capacities of hot-rolled and welded built-up I-shaped girders.

Past studies examined the flexural response of welded I-shaped girders, with some proposing design recommendations taking into account their expected buckling response. Ji et al. (2022) performed full-scale experimental testing to examine the LTB resistance of compact ($h/w < 60$ and $b/t < 8.5$, where b and t are the width and thickness of flanges, respectively) I-shaped welded steel girders and found that the current design equations can accurately predict the moment resistance of compact welded steel girders that fail in either the elastic or inelastic LTB mode. An experimental study was performed by Slein et al. (2023) to improve the inelastic LTB equations in AISC 360 for the design of I-shaped members. Phillips et al. (2023) conducted full-scale testing of I-shaped welded steel girders and showed that the AISC 360 design equations overestimate the flexural resistance of specimens because of web distortion not being properly accounted for by this standard and the direct scaling of the beam design curve by the moment gradient factor C_b. It was also confirmed that the strength overprediction is exacerbated as the web slenderness ratio increases.

The adequacy of the current LTB provisions in North American steel and bridge design standards for estimating the moment resistances of I-shaped welded steel girders with slender webs was evaluated using full-scale experimental testing, particularly, the influence of web distortion effects on the flexural capacity of such girders were interrogated using the test data and recommendations were made to indirectly address this effect in design. Four I-shaped welded steel girder specimens with $d/b \approx 2.5$, where d is the overall depth of the section, $h/w \approx 90$ and $5.5 < b/t < 8.6$ were experimentally tested. The web depth-to-thickness ratios of the specimens are close to the Class 2/3 (as per CSA S16), or compact/noncompact (as per AISC 360), boundary. Two plate cutting methods, including plasma and oxy flame, typically used in the construction of building and bridge girders in North America were evaluated.

2.2 Test Specimens and Setup

The test matrix, showing measured dimensions and cross-sectional properties of the specimens, is presented in Table 1. The specimens are labeled as the letter 'G' (for girder), followed by the first digit of section depth in mm – flange width in mm – flange thickness in mm – section class (in design) – cutting method ('p' for plasma and 'f' for oxy flame). A is the cross-sectional area, J is the St. Venant torsional constant, C_w is the warping constant, and L/r_y is the member slenderness ratio with respect to the weak-axis radius of gyration, r_y, where L is the unbraced length of the girder. The test specimens shown in Fig. 1a were designed to span an unbraced length of L = 9.75 m (32 ft) between end supports. The test specimens were subject to an approximated distributed load involving eight equally-spaced point loads applied to the girders at 1.22 m (4 ft) intervals along the girder length. Initial geometric out-of-straightness, including initial sweep, camber, and cross-sectional twist along the span length, and measured residual stresses are reported in (Twizel et al. 2023) and Unsworth et al. (2020), respectively. On average, the maximum absolute initial top (compression) and bottom (tension) flange sweeps are $L/2000$ and $L/4110$, respectively, both lower than the maximum fabrication tolerance of $L/1000$ set by CSA W59-18 (CSA 2018) and AWS (2015).

Table 1: Test specimen measured properties, moment capacities and buckling modes.

Specimen ID	d	b	t	w	A	J	C_w	d/b	b/t	h/w	L/r_y	M_{max}	M_{max}/M_p	Buckling Mode
	mm	mm	mm	mm	mm^2	$\times 10^3$ mm^4	$\times 10^9$ mm^6					kN-m		
G9-360-32-3-p	898	353	31.6	9.87	30581	7734	43548	2.5	5.6	84.6	112	1852	0.47	Inelastic
G9-360-32-3-f	900	351	31.7	9.91	30572	7749	43197	2.6	5.5	84.4	113	2002	0.50	Inelastic
G9-360-25-3-f	900	359	24.9	9.90	26294	3980	36742	2.5	7.2	85.8	114	1645	0.48	Elastic
G9-430-25-3-f	902	429	25.1	9.81	29895	4795	63561	2.1	8.6	86.8	93	2408	0.60	Inelastic

A photograph of the experimental test setup including one of the test specimens and test setup components is shown in Fig. 1b. The point loads were applied on the top flange of the specimens. The combined height of the testing fixture resulted in a load height of 178 mm above the top surface of the top flange. Simple supports were provided at the specimen ends, where the girders were free to displace longitudinally but prevented from displacing vertically or laterally. At the supports, the member was free to displace rotationally both in- and out-of-plane; only the rotation about the longitudinal axis (twist) was prevented. The simply-supported boundary condition was achieved using a set of rollers, topped by a load cell, then a knife edge. Four lateral braces were installed at each support to prevent lateral movement and twist, while allowing the ends to freely rotate in and out of the plane. The specimen was also free to displace longitudinally and warp. Full-depth bearing and intermediate transverse stiffeners were designed in accordance with CSA

S16 requirements. Additional details regarding the design of the test setup and fixtures can be found in Ji et al. (2022). The test was performed in a load-controlled manner, with a rate varying between 0.5 and 1.0 kN/GLS/s to capture elastic response, buckling point and post-buckling response.

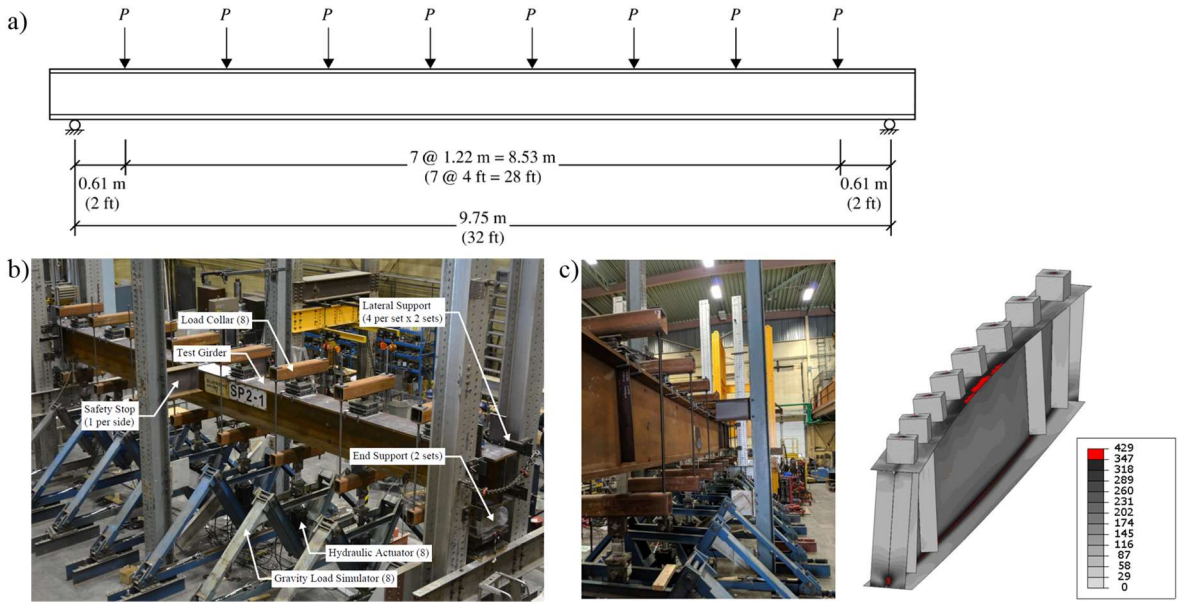

Figure 1: a) Specimen layout and load configuration; b) Test setup; c) G9-360-32-3-f final buckled shape from the experiment versus finite element analysis (stresses in MPa).

Given that member instability with significant out-of-plane deformation and cross-sectional twist is expected in this test program, it is crucial to keep the applied load vertical throughout the test as the member displaces laterally and twists in the post-buckling range. This was achieved using a set of Gravity Load Simulators (GLSs), shown in Fig. 1b, designed to act as a mechanism in the plane parallel to the cross-section of the girder to accommodate deformation of the member, as it buckles, without creating lateral restraint. The GLS is a pin-jointed mechanism designed for testing structures experiencing sideway movements under a vertical load (Yarimci et al. 1967). In this test program, the GLSs were designed to accommodate a lateral displacement of 400 mm and a force capacity of 385 kN. Another challenge when evaluating the buckling response of steel girders was to keep the load application point at the girder shear center to avoid adjusting for load height when comparing the test moments with code predictions as both CSA S16 and AISC 360 beam design equations assume transverse loads are applied at the shear center. Applying transverse loads at the shear center of the specimens was not feasible in the laboratory due to the lateral movement expected as the member buckles out-of-plane, and the potential stress concentration in the thin web of the specimens tested here. The loads were therefore applied 178 mm above the top surface of the top flange due to the combined height of the testing fixture, including a roller assembly and a sacrificial steel plate to avoid damaging the roller. To achieve the respective shear center loading with the intent of conducting a fair comparison between the test moments and those from design equations corresponding to girders with transverse loads applied at the shear center, the finite element model (FEM) of the specimens was developed to mimic the test setup and estimate the test moments by explicitly modeling the roller assemblies atop the girders. This numerical model was then refined to create a loading condition where transverse loads are applied at the shear center and used to estimate moment capacities corresponding to that predicted by the code equations.

2.3 Experimental Results

The dominant failure mode of all tested girders was member lateral buckling. No evidence of local buckling or shear buckling was visually observed during the experiments. Table 1 gives the maximum observed bending moment, M_{max}, the maximum moment normalized by the measured plastic moment capacity of the cross-section, M_{max}/M_p, and the mode of buckling. The difference in the magnitude of rotation experienced by the top and bottom flanges at buckling and in the post-buckling range was used as a criterion to identify web distortion. When the web of an I-shaped member distorts, the effective St. Venant torsional stiffness is reduced, and a lower moment resistance (1 – 9% lower) than that of an LTB failure is produced (White and Jung 2007). The reduction in the flexural strength due to web distortion can be significant in girders with relatively stocky flanges (i.e., low b/t) and flexible webs (i.e., high h/w). For the specimens tested here, a noticeable difference was observed in the top and bottom flange twist at buckling with a mean cross-sectional twist of 1.0°. This value is nearly three times the mean value of the cross-sectional twist observed for I-shaped welded girders with stockier webs ($h/w < 60$) reported in (Ji et al. 2022). These results suggest that web distortion likely occurred as LTB took place, indicating that the specimens tested here failed due to the combined LTB and LDB modes.

2.4 Evaluation of Design Equations

The flexural resistance of I-shaped welded steel girders with $d/b \approx 2.5$ and $h/w \approx 90$ predicted using CSA S16 and AISC 360 were evaluated using the corroborated FEM where transverse loads are applied at the shear center. Refer to Twizell et al. (2023) regarding the details of the FEM. The moment capacities predicted by the FEM when loaded at the shear center, $M_{FEA\text{-}SC}$, were compared to the associated code predictions by CSA S16-19, M_{CSA} (Clause 13.3.1a), and AISC 360-16, M_{AISC} (Section F2) in Table 2. Note that FEM moments were corrected using a mean bias factor of 1.1, computed as the mean value of the ratios between the test moment and numerical moment when the load is applied 178 mm above the top flange, to account indirectly for the slightly lower strength and stiffness of the numerical model as compared to the specimens.

Table 2: Moment capacities predicted under shear-center loading versus the moment resistances predicted by CSA S16 and AISC 360.

Specimen ID	Moment, $M_{FEA\text{-}SC}$ (kN-m)	CSA S16				AISC 360			
		Moment, M_{CSA} (kN-m)	FEA-to-Code Ratio	Moment, $M_{CSA\text{-}J=0}$ (kN-m)	FEA-to-Code Ratio $J = 0$	Moment, M_{AISC} (kN-m)	FEA-to-Code Ratio	Moment, $M_{AISC\text{-}J=0}$ (kN-m)	FEA-to-Code Ratio $J = 0$
G9-360-32-3-p	2446	2907	0.84	2379	1.03	2986	0.82	2390	1.02
G9-360-32-3-f	2596	2892	0.90	2351	1.10	2967	0.88	2360	1.10
G9-360-25-3-f	2233	2338	0.95	1999	1.12	2372	0.94	2003	1.11
G9-430-25-3-f	3078	3272	0.94	3101	0.99	3321	0.93	3142	0.98

In Table 2, the code-specified moments are unfactored and calculated using the measured cross-sectional properties and yield stresses with an equivalent moment factor prescribed by the respective design method for the uniformly distributed loading condition. A FEA-to-code ratio lower than unity indicates that the code equation overestimates the anticipated moment resistance and a FEA-to-code ratio exceeding one indicates an understimation. Referring to Table 2, significant discrepancies were observed between M_{CSA} and $M_{FEA\text{-}SC}$ for the specimens. The moment capacities predicted numerically were consistently overestimated by the code equation, suggesting that the CSA S16 design equation may be inappropriate for estimating the buckling

resistance of girders of these proportions, as they likely buckle in a combined LTB and LDB mode. On average, the FEA-to-code prediction ratio is 0.91 for CSA S16, with a coefficient of variation of 5.6%. A similar trend was observed for the AISC 360 predictions. The comparisons between M_{AISC} and $M_{FEA\text{-}SC}$, as shown in Table 2, indicate that AISC 360 also overestimates the resistance of the specimens with a mean FEA-to-code ratio of 0.89, a coefficient of variation of 6.2%.

Table 2 also includes CSA S16 and AISC 360 moment capacities recalculated, $M_{CSA\text{-}J=0}$ and $M_{AISC\text{-}J=0}$, assuming the St. Venant constant $J = 0$ as a conservative estimate of the effect of combined LTB and LDB on the flexural resistance of I-shaped girders (Winter 1943; White and Jung 2007). Comparing the moment resistances for shear center loading to the modified design predictions (when $J = 0$), $M_{CSA\text{-}J=0}$ and $M_{AISC\text{-}J=0}$, shows a mean FEA-to-code prediction ratio of 1.06 for CSA S16 with a coefficient of variation of 5.7%, and 1.05 with a coefficient of variation of 6.0% for AISC 360. This suggests that the flexural resistance of I-shaped steel girders having webs with slenderness similar to those tested here ($h/w \approx 90$) can be computed assuming $J = 0$ as a simple approach to estimating the combined LTB and LDB. Further studies are needed to enhance the accuracy of predicting the moment resistance when combined LTB and LDB modes occur. In particular, modified beam design equations should be developed to account for this combined mode, leveraging additional experimental and numerical simulation as it becomes available.

3. Gerber Framing System

3.1 Background

The cantilever-suspended-span construction, also known as Gerber roof framing system, is widely used in the construction of single-story steel buildings in North America. This roof framing system involves a series of I-shaped girders that extend beyond the column as cantilevers (back span) and drop-in segments (suspended spans) connected at the cantilever ends through a shear connection in alternate bays, as shown in Fig. 2. Open-web steel joists (OWSJs) are often used as secondary framing members of this roofing system as shown in Fig. 2a. The girders of the Gerber systems are subjected to upward or downward transverse loads applied on their top flange and often near the shear centre at the cantilever tips due to dead, snow and wind loads. Design engineers often prefer the Gerber framing system over simply-supported spans lacking continuity over vertical supports because 1) a balanced moment is achieved between spans, 2) drop-in beams are often lighter than those of standard framing (Fig. 2), 3) deflections in interior spans are reduced due to continuity, 4) simple connections are used to connect the beams, and 5) erection of the structure is accelerated.

Figure 1: a) Steel-framed roof of a retail store in Edmonton, Canada; b) Typical cantilever-suspended-span construction.

Despite the widespread use and benefits of the Gerber system in steel buildings across North America, little guidance on the design of these systems is provided by current steel design standards in both Canada, CSA S16, and the United States, AISC 360-22, or by the Structural Stability Research Council (SSRC) Guide to Stability Design Criteria for Metal Structures (Ziemian 2010). Moreover, several collapses of buildings with the Gerber framing system have been reported in the past, including the roof collapse in a Burnaby, BC supermarket in 1988 (Closkey 1988), collapses in warehouse buildings in Texas in 2011, in Halifax in 2015 and in Montreal in 2019 (Metten 2019), which necessitates the evaluation of the stability response of overhanging beams and assessment of proper bracing strategies and details.

Full-scale physical testing of overhanging girders exposed to different bracing and loading conditions anticipated in the construction of the Gerber roof framing system is crucial for understanding the stability response of such girders and for developing a design approach that systematically accounts for influential parameters affecting the flexural capacity of the system. A full-scale experimental program was therefore developed to evaluate the stability response of single-overhanging I-shaped steel girders under different loading and restraint conditions often seen in practice. The test results were used in combination with the corroborated finite element simulations to develop a regression-based equation to predict the flexural capacity of single-overhanging beams.

3.2 Test Specimens and Setup

The test specimens comprised single-overhanging girders, each 10.8 m long, with four equally spaced point loads (every 1.8 m) applied at the back span and an additional point load applied at the cantilever tip, resulting in a 9m-long back span and a 1.8m-long cantilever. A total of 14 W410×85 girders were selected based on finite element simulation results (Esmaeili et al. 2021) to represent five different restraint conditions and three different loading scenarios. The restraint conditions included 1) unbraced cantilever tip and laterally restrained back span at their top flange, 2) laterally restrained cantilever tip and back span at their top flange, 3) laterally braced cantilever tip at both the top and bottom flanges and laterally restrained back span at the top flange, 4) unbraced cantilever tip, laterally braced back span at the top flange at all load locations, and laterally restrained bottom flange at the first load point from the fulcrum support, and 5) laterally restrained cantilever tip at both the top and bottom flanges, laterally restrained back span at the top flange at all load locations, and laterally restrained bottom flange at the first load point from the fulcrum support. Each bracing condition is tested under various load ratios defined as the ratio between one of the point loads on the back span to the point load applied at the cantilever tip to create the desired bending moment gradient anticipated under various combinations of dead, snow and wind loads. Three load ratios, including 0.25, 0.38 and 0.80, were considered.

The test setup was designed to accommodate the expected girder displacements and rotations based on finite element simulations reported in (Esmaeili et al. 2021) and recommendations by the SSRC Guide Technical Memorandum No. 9 on flexural testing. Fig. 3a shows the test setup for the fourth group of restrain conditions described above. Further information regarding the test matrix and test setup design can be found in Essa et al. (2024).

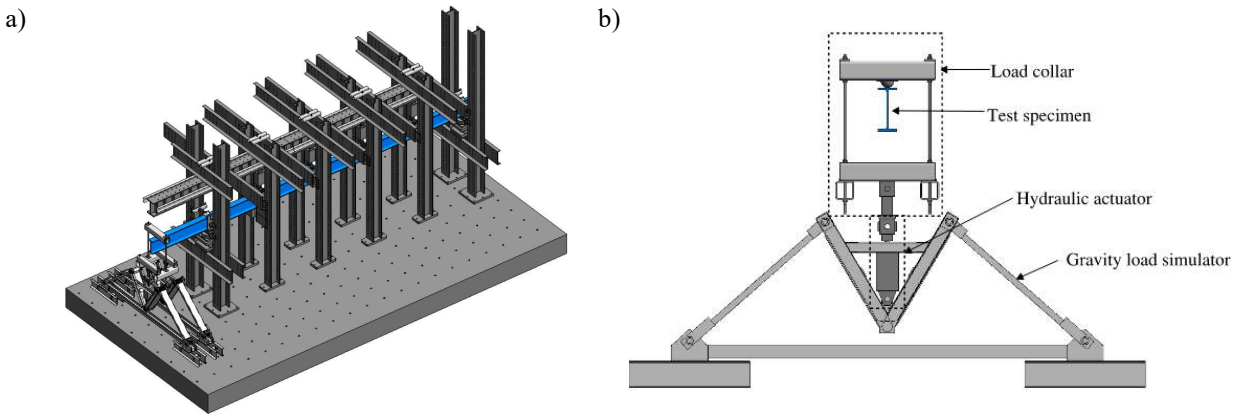

Figure 3: a) Experimental test setup (test specimen in blue); b) Gravity load simulator at unbraced cantilever tip.

The simulation of various restraint conditions, including laterally braced flanges in the back span, free or laterally braced cantilever tip, and torsionally braced supports, posed challenges in designing the test setup. To create a condition where the flanges are laterally restrained at the load application points, U-shaped bracket plates were used at each lateral bracing point. A cylindrical Acetal piece was then installed on the flange of the test girder to reduce the frictional force that could be developed between two steel surfaces as the girder moves in the vertical and longitudinal directions. At each braced point, a hydraulic actuator was installed to apply the vertical load on the top flange of the beam through a semi-cylindrical bearing with its axis aligned with the longitudinal axis of the specimen, allowing for cross-section twist while maintaining a stable mechanism with the pin-ended hydraulic actuator. To reproduce an unbraced cantilever tip, a set of two GLSs and two hydraulic actuators with a load collar as shown in Fig. 3a were used. As described earlier, the GLS can freely displace up to 400 mm in either direction while maintaining a nearly vertical point load as the hydraulic actuators apply a downward concentrated load to the top flange of the specimen and the load collar provides accommodations for cross-section twist using a hemispherical bearing installed on the top flange of the specimen (Fig. 3b). However, in the tests experiencing LTB, and in turn large lateral displacement and cross-sectional twist, at the cantilever, lateral out-of-plane deformation of the cantilever tip was accommodated in part by the flexural bending of the threaded rods of the load collar, which were not designed for such deformation. In the future, efforts should be directed toward minimizing redundancy in the load collar to prevent it from experiencing unintended lateral deformation, thus allowing the GLS to accommodate the lateral deformation. Another challenge encountered in the test was the unintended rotational restraint about the vertical axis developed by the vertical support assembly and the torsional stiffness of the U-shaped side plates used to laterally brace the girder at the vertical support locations, which likely caused an additional partial warping restraint at the fulcrum support, where significant warping deformations are expected when the cantilever experiences LTB. In future experiments of similar nature, it may be beneficial to use slender steel bars for lateral bracing of the specimen at the vertical support location, preferably attached to the girder web.

3.3 Experimental Results

The results of the experiments confirmed two main failure modes: 1) plastic hinging at the back span as shown in Fig. 4a or at the fulcrum support, and 2) inelastic LTB at the cantilever as shown in Fig. 4b. In general, higher load ratios, e.g., 0.85, promoted plastic hinging and lower load ratios, e.g., 0.25, and lack of lateral support at the cantilever tip, either on both flanges or on the bottom

flange, resulted in LTB at the cantilever. Moreover, the additional lateral brace on the bottom flange of the back span (at the load point closest to the fulcrum support), bracing conditions 4 and 5, did not have a noticeable impact on the moment capacity of the girder when the cantilever remained unbraced. This suggests that providing braces at the top and bottom flanges at the cantilever tip or even at the top flange at the cantilever tip is more effective compared to bracing the back span closest to the fulcrum at the bottom flange.

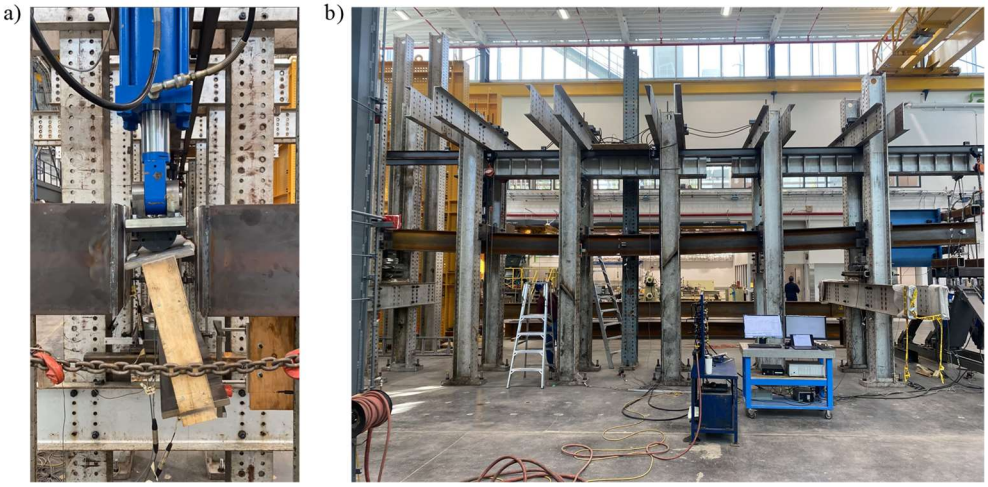

Figure 4: a) Lateral-torsional buckling of Specimen 2-0.38 at the cantilever; b) Plastic hinging of Specimen 4-0.80 at back span.

3.4 Proposed Design Method

A novel regression-based method is proposed on the basis of extensive numerical simulations using the corroborated finite element model of overhanging steel girders to determine their flexural capacity. Based on the proposed method, the factored moment resistance of an overhanging beam is estimated as $M_r = \varphi\Omega_2 M_p \leq \varphi M_p$ where φ is the resistance factor equal to 0.9, Ω_2 is the moment modification factor that accounts for 1) the elastic LTB capacity of the girder assuming an unbraced length equal to the length of back span, 2) the moment gradient within the back span, 3) lateral bracing conditions at the cantilever tip, including laterally free, laterally braced at the top flange and laterally braced at both flanges and 4) web slenderness ratio to account for the influence of distortional buckling on the flexural capacity of overhanging beams. Details of the proposed method, including the design tables providing the Ω_2 coefficients for potential lateral restraint conditions expected in practice, will be presented in future relevant publications.

4. Concentrically Braced Frames

4.1 Seismic Response

Steel Concentrically Braced Frames are widely used as the lateral load-resisting system of multi-story buildings. Under lateral seismic loads, the lateral roof displacement may not be distributed evenly between the stories as their braces experience nonlinear response through tensile yielding and buckling, resulting in the concentration of lateral inelastic displacements in one or some of the stories (Tremblay 2000; MacRae et al. 2004). This unsatisfactory response is more pronounced in tall (Tremblay and Lacerte 2002; Tremblay and Poncet 2004; Redwood et al. 1991; Lacerte and Tremblay 2006) and existing CBFs (Balazadeh-Minouei et al. 2017), those with heavy gravity loads imposing large P-Δ effects. Non-uniform distribution of frame lateral displacements in CBFs

stems from their poor performance in redistributing inelastic demands over the height mainly due to inherent poor hysteretic response of diagonal braces when buckling in compression, which significantly reduces storey shear resistance in the story experiencing buckling and yielding, thus discouraging yielding to develop in adjacent floors (Tremblay 2003; MacRae et al. 2004; Lai and Mahin 2015; Imanpour et al. 2016a; Uriz and Mahin 2008).

In multi-tiered concentrically braced frames not specifically designed for multi-tier response, damage concentration occurs in one of the braced panels along the frame height and can potentially cause column buckling due to appreciable in-plane bending induced in the column in the presence of a large axial compression force and/or brace fracture due to significant deformation demands induced in the braces of the tier where brace tensile yielding takes place (Fig. 5a). Past numerical studies performed to examine the seismic response of multi-tiered steel CBFs, designed neglecting special seismic design provisions introduced for the first time in 2009 in CSA S16 and in 2016 in AISC Seismic Provisions, confirmed that brace tensile yielding tends to occur in only one of the tiers leading to large lateral deformation in that tier and significant in-plane bending in the columns (Imanpour et al. 2016a; 2016b; Imanpour and Tremblay 2016; Cano and Imanpour 2020). Column instability observed in numerical analyses when the column base is assumed to be pinned consisted of in-plane buckling about section weak-axis over the first tier followed by out-of-plane buckling about section strong-axis over the full frame height as shown in Fig. 5b for a two-tiered CBF designed to 2010 AISC Seismic Provisions for Structural Steel Buildings, AISC 341 (AISC 2010a). A pseudo-dynamic hybrid test program was developed to examine this unique biaxial buckling mode, verify the stability response of multi-tiered CBFs under seismic loading, validate the numerical models used in the past to develop seismic design procedures that have been implemented in North American design guidelines.

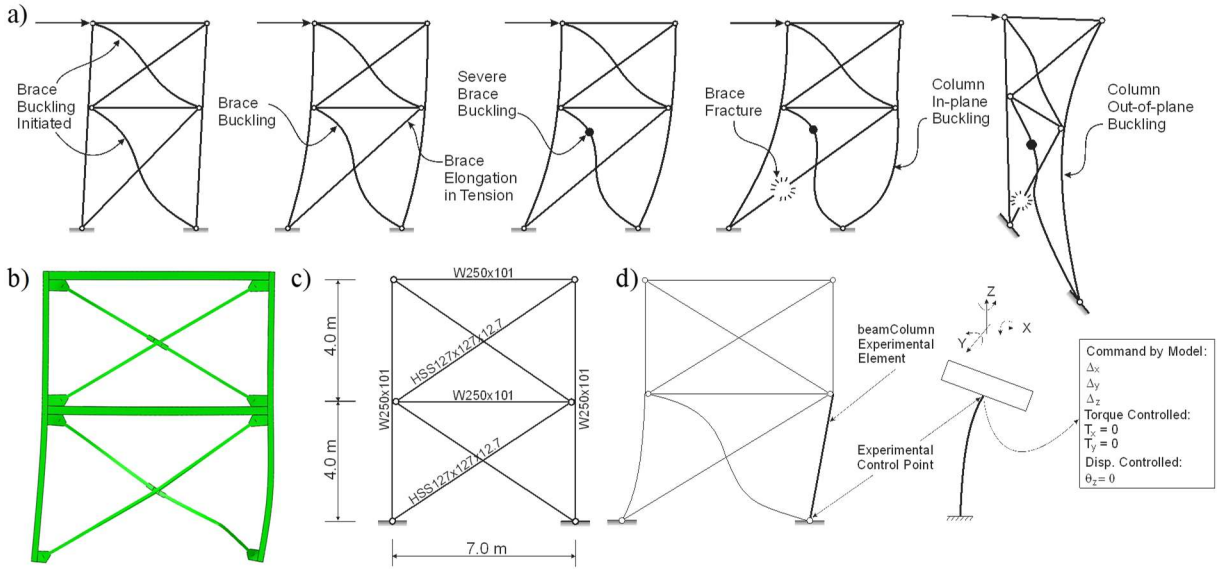

Figure 5: a) Anticipated seismic response of multi-tiered CBFs not designed for multi-tier response; b) Buckling of the right column in the first tier segment of a two-tiered CBF; c) Two-tiered concentrically braced frame selected for hybrid testing; and d) Hybrid test numerical and experimental substructures.

4.2 CBF Selected and Experimental Program

A two-tiered concentrically braced frame shown in Fig. 5c was selected to evaluate using hybrid testing the stability response of steel multi-tiered CBFs. The frame acts as the seismic force-

resisting system of an 8m-tall single-story industrial building located on Class D site in coastal California. The design of the frame as a Special Concentrically Braced Frame (SCBF) system was performed in accordance with ASCE 7-10 (ASCE 2010), 2010 AISC Specification for Structural Steel Buildings, AISC 360 (AISC 2010b) and 2010 AISC 341. Since the frame does not comply with the special design requirements for multi-tiered braced frames in 2016/2022 AISC 341, it was expected that the column physically simulated in the laboratory would experience buckling due to uneven distribution of frame inelastic deformation in Tier 1, which is the week tier of this frame where brace tensile yielding took place. Additional details on the loading and seismic design of the frame specimen in (Imanpour et al. 2022). Note that the building height and the seismic weight were adjusted such that the height of the first-tier column segment corresponds to the available 4 m test height of the testing machine.

A multi-axis pseudo-dynamic (slow) hybrid test was performed to examine the seismic stability of the two-tiered braced frame specimen with the first-tier W250×101 column segment being experimentally tested in the laboratory while the rest of the frame was modelled numerically in the *OpenSees* program (McKenna et al. 2010), as shown in Fig. 5d. The schematic of the hybrid loop is shown in Fig. 6. The development of the numerical substructure for the hybrid test is described in detail in (Imanpour et al. 2018). The capacities of the testing machine and control system used to perform the test can be found (Imanpour et al. 2022). An integration algorithm with a fixed number of iterations was used to solve the nonlinear dynamic problem during the test. The gravity loads were first applied to the frame in the numerical model while the portion of the gravity loads resisted by the specimen was simultaneously imposed to the column specimen in the laboratory. The gravity analysis was followed by a dynamic response history analysis under the 1992 Landers - Yermo Fire Station earthquake record.

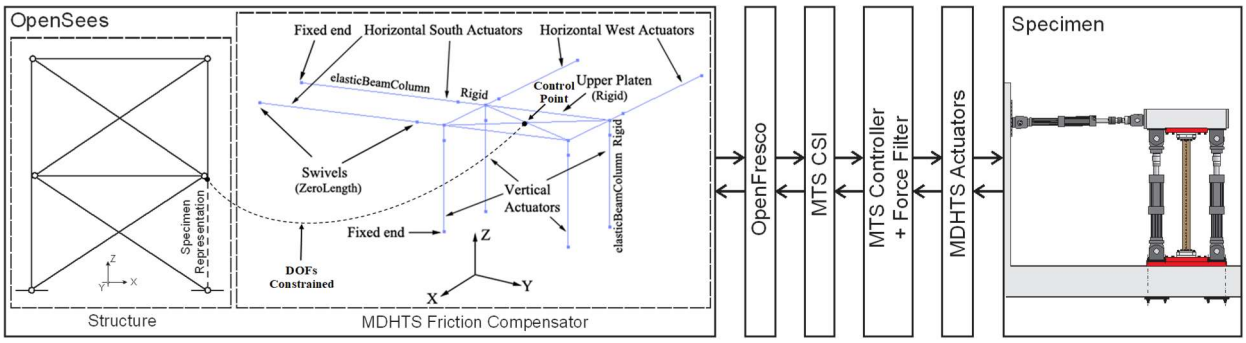

Figure 6: Hybrid simulation loop including the friction compensation tool.

4.3 Hybrid Testing Challenges

A major challenge encountered during multi-axis hybrid testing of the two-tiered CBF was the development of friction forces in the actuator swivels of the testing system as they interact to achieve imposed displacements or rotations sent by the numerical substructure. Unintended friction resulted in measured forces that were not consistent with the expected forces, which produced inaccurate displacement commands by the hybrid computational model, propagating errors through the test. A friction compensation technique was developed to mitigate the detrimental effects of the friction forces generated in the testing system on the hybrid test. This technique involved including in the computational model the three-dimensional model of the testing system that was constructed in the *OpenSees* environment as shown in Fig. 6. The role of the numerical model of the testing system acting in parallel with the braced frame numerical model in the same *OpenSees* model was to

generate negative forces neutralizing the effects of friction. This is achieved by assigning to the springs representing actuators' swivels a moment-rotation response associated with the friction forces measured in the translational and rotational degrees-of-freedom (DOFs) of the testing system and by constraining these DOFs in the testing system's control point to those of the node representing the specimen in the numerical model of the structure (Fig. 6). Thus, the feedback forces along each DOF were corrected to provide accurate force feedback signals representative of the specimen resistance in the test. The only limitation of this technique is that it neglects the influence of the load applied by vertical actuators on the friction resistances generated in their swivels.

4.4 Hybrid Test Results

Figure 7 shows the results of the hybrid test, including tier drifts, column axial force-axial displacement response, and column lateral in-plane and out-of-plane displacement responses at the strut level. As shown in Fig. 7a, large lateral deformation develops in Tier 1 compared to the adjacent noncritical tier due to brace tensile yielding that initiates in Tier 1 at 0.5% story drift, which led to the reduction of the story shear resistance in that tier, preventing brace tensile yielding in Tier 2 during the test. As shown, drift in Tier 1 increases as the roof displacement augments, whereas drift in Tier 2 remains below 0.5% as the braces of that tier did not experience tensile yielding. This response induced in-plane bending in the columns with the peak taking place at the strut level which, in the presence of a large axial compression force, led to buckling of the left column in Tier 1 at t = 16.5 s of the ground motion time (Fig. 7b). Column buckling involved appreciable in-plane and out-of-plane lateral displacements at the strut level, as shown in Figs. 7c and 7d, respectively. This was followed by a loss of the axial load-carrying capacity of the column (Fig. 7b). The final deformed shape of the specimen at t = 16.5 s is shown in Fig. 7e.

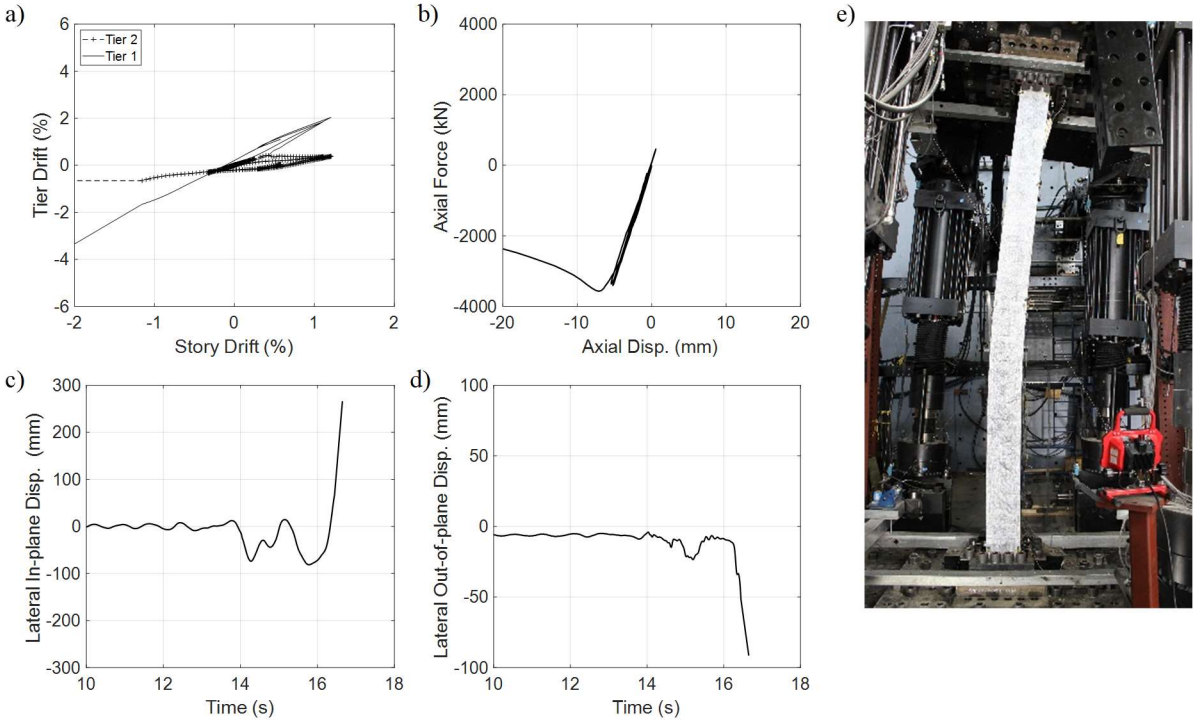

Figure 7: Hybrid testing of two-tiered CBF under the 1992 Landers - Yermo Fire Station record: a) Tier drifts; b) Column axial force-axial displacement; c) Column lateral in-plane displacement at the strut level (first 10 seconds not shown); d) Column lateral out-of-plane displacement at the strut level (first 10 seconds not shown); and e) Column buckled shape at t = 16.5 s.

5. Moment Resisting Frames

5.1 Stability of Fixed-base Columns

Low-to-mid-rise steel MRF buildings in North America often consist of wide-flange columns resisting gravity loads, and lateral seismic loads by primarily bending about their strong-axis. First-story fixed-base columns in steel MRFs expected to develop plastic hinging at their base should have sufficient strength and remain stable when the beams reach their probable flexural resistances. The columns, and MRF beams, should also possess sufficient flexural stiffness to ensure that frame inter-story drifts do not exceed the drift limit specified by the building code, e.g., 2.5% per the National Building Code, NBC, of Canada (NRC 2020). Columns with deep wide-flange sections (i.e., $d/b \approx 2.0$) are therefore ideal in MRF design since they offer higher lateral stiffness and flexural capacity compared to square wide-flange sections (i.e., $d/b \approx 1.0$) with the same weight.

Extensive experimental and numerical research has been conducted over the past decade to understand the cyclic response of steel wide-flange columns, characterize their failure modes and develop seismic design requirements for enhancing the seismic response of steel MRFs (Elkady and Lignos 2015, 2017, 2018a, Ozkula et al. 2017a, 2017b, 2021; Uang et al. 2019). These studies confirmed that the columns with large global slenderness ratios ($L_b/r_y \geq 80$, where L_b is the unbraced length of the column) may be prone to out-of-plane instability, including weak-axis flexural buckling or lateral-torsional buckling, at large story drifts. It was also found that column cyclic response is a function of its end conditions. For instance, the columns having a fixed-flexible end condition experienced less severe local buckling at their flexible end. Despite significant advancement in understanding the cyclic response of steel wide-flange columns, the effect of the limit states observed in past studies on member stability response has not yet systematically been quantified. Furthermore, seismic design recommendations in the framework of the Canadian design practice that account for the combined effects of the parameters affecting the stability condition of fixed-base wide-flange columns are required. To address this need, a research study was initiated to evaluate the stability response of wide-flange columns located in the first story of Ductile steel MRFs under seismic loading and propose enhanced stability design recommendations for such columns in the framework of the Canadian steel design standard.

5.2 Parametric Study Matrix and Finite Element Model

A prototype five-story office building with perimeter MRFs located on Site Class C in Vancouver, British Columbia was selected. Loading was performed in accordance with the 2015 NBC (NRC 2015). One of the MRFs was selected and designed as a Ductile (Type D) steel MRF in accordance with 2019 CSA S16 seismic provisions. Beam-to-column moment connections consisted of reduced beam section (RBS) connections designed following the CISC Moment Connections for Seismic Applications (CISC 2014). Refer to Islam and Imanpour (2022) for detailed design information.

The FEM of a wide-flange column isolated from the first story of the selected MRF was developed in the *Abaqus* program (Simulia 2011). This model consisted of a wide-flange column constructed using shell elements (S4R) with a uniform mesh size of 25 × 25 mm and a wide-flange beam extending between the column top end and beam mid-span simulated using wire elements. The beam was intended to simulate the in-plane flexibility of the beam-to-column joint while representing flexural demands transferred from adjoining beams to the column at the joint. Additional information

regarding modeling assumptions and material parameters can be found in (Islam and Imanpour 2022).

The FEM of the column was subjected to a constant axial compression force, strong-axis (in-plane) displacement and weak-axis (out-of-plane) bending moment histories. The cyclic loading protocol proposed by 2016 AISC 341 (AISC 2016a) was used to simulate the in-plane cyclic displacement anticipated under seismic loads. The maximum story drift angle applied to the column was 4%, which can conservatively represent the NBC design-level hazard. The column was also subjected to a constant gravity-induced axial compression C_f equal to $0.15AF_y$ (where F_y is the specified yield strength of steel), representing an axial load level observed in typical Type D MRFs. Past experiments on isolated wide-flange columns showed that deep columns also experience out-of-plane deformation at large story drift ratios when severe local buckling develops near their base. This out-of-plane response may be exacerbated by the out-of-plane deformation generated by the adjoining beams, after plastic hinging, and upper-story columns. In this study, an MRF subassembly consisting of the exterior bay plus half of the adjacent interior bay isolated from the selected MRF was numerically modelled and subjected to a set of ground motion accelerations to reproduce the out-of-plane bending demand developed at the top end of the first-story MRF column under seismic loading. The weak-axis bending history represents the envelope of out-of-plane moments from the time history analysis of the subassembly model. Further information regarding the subassembly model and development of the out-of-plane moment history can be found in (Islam and Imanpour 2023).

A total of 26 Class 1 ($b/t \leq 7.8$ and $h/w \leq 55$) steel wide-flange columns – that also meet the width-thickness ratio for highly compact members in 2016 AISC 341, except for W530×150 and W610×174 where the flange width-to-thickness ratio slightly exceeds the AISC limit – representing interior MRF columns was selected to evaluate the column stability response. The column database included deep sections ($d/b \geq 1.74$), W530×150, W530×182, W610×125, W610×153, W610×174 and W610×217 profiles, and a square ($d/b \approx 1.0$) W360×237 profile. Four unbraced heights L_b = 3.3, 4.3, 5.3, and 6.3 m were considered for deep members, while the W360×237 column had L_b = 4.3 and 6.3 m. The parametric study matrix was developed such that while creating a wide range of column stability influential parameters, including the global slenderness ratio $42.2 \leq L_b/r_y \leq 127.3$, section aspect ratio $0.96 \leq d/b \leq 2.72$, flange width-to-thickness ratio $6.56 \leq b/t \leq 7.68$, and web width-to-thickness ratio $17.0 \leq h/w \leq 48.1$, they can represent practical and available members used in low-to-mid-rise steel MRF buildings in North America, with the emphasis on deep sections, which favor a more economical MRF design.

5.3 Column Stability Response

Two failure modes dominated the stability response of the columns that failed – identified when the flexural strength falls below 50% of the plastic moment capacity of the column – under applied cyclic loading: 1) out-of-plane buckling at the column base due to severe local buckling, and 2) member buckling along the length of the column. Both failure modes are accompanied by severe strength degradation leading to the loss of column load-carrying capacity. Figs. 8a and 8b show an example of out-of-plane buckling at the base observed for the 4.3m-long W610×153 column and an example of member buckling observed for the 5.3m-long W610×153 column, respectively.

Stocky columns exhibited no noticeable strength degradation owing to their stable cyclic response with minor web and flange local buckling at the base (Newell and Uang 2008), even in the presence of fairly considerable weak-axis bending demands. Deep columns exhibited severe strength degradation compared to their expected plastic moment. The flexural strength of the column degrades as both L_b/r_y and d/b increase. In general, shorter columns, L_b = 3.3 and 4.3 m, that failed exhibited large axial shortening (> 2% times the length of the column) and out-of-plane displacement near the base plastic hinge (> 2% times the length of the column) accompanied by large strength deterioration, promoting column out-of-plane buckling at the base due to severe local buckling near the plastic hinge location, i.e., the first failure mode described above. Whereas longer, 5.3 m and 6.3 m columns underwent a large cross-section twist angle (> 0.10 rad.) near the base plastic hinge plus large out-of-plane deformations propagated over the member height; this was accompanied by large strength deterioration, suggesting a tendency for member buckling, i.e., the second failure mode described above.

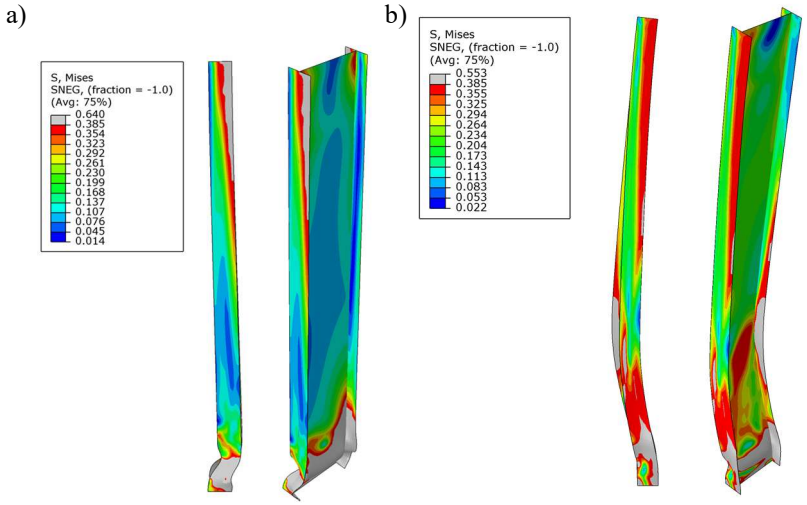

Figure 8. In-plane and out-of-plane deformed-shape and von Mises stress distribution at the end of the analysis of columns under an axial load of $0.15AF_y$: a) W610×153 column failing by out-of-plane buckling at the base; b) W610×153 column failing by member buckling.

5.4 Stability Design Recommendations

On the basis of the column stability parametric study and considering the correlation between the column response parameters and the geometrical properties, including the member global slenderness ratio L_b/r_y and cross-section aspect ratio d/b, and the axial load ratio C_f/AF_y, an empirical equation is proposed for evaluating the out-of-plane stability of fixed-base wide-flange columns of Ductile steel MRFs:

$$\left(\frac{C_f/AF_y}{0.15}\right)^{1.4}\left[\left(\frac{L_b/r_y}{108}\right)^2+\left(\frac{d/b}{3}\right)^2\right]\le 1.0 \qquad (1)$$

The proposed equation couples the global slenderness ratio, cross-section aspect ratio and axial load ratio to predict the stability condition of wide-flange columns with base plastic hinging.

6. Conclusions

This paper presented the results of experimental testing and numerical simulations for I-shaped welded steel girders, overhanging steel beams, steel concentrically braced frames, and steel moment-resisting frame columns. The stability response of these systems under anticipated loads, gravity, wind, seismic and/or the combination of these loads, were described and proposed stability design recommendations were presented. The key findings of this study are summarized as follows:

- Full-scale testing and detailed numerical simulation of structural systems, subassemblies and connections provide an enhanced understanding of complex structural stability problems and help develop improved stability design guidelines for steel systems under gravity, wind and earthquake loads.
- I-shaped welded girders with $d/b \approx 2.5$ and web slenderness ratios near the CSA S16 Class 2/3, or AISC 360 compact/noncompact boundary ($h/w \approx 90$) fail in a combined LTB and LDB mode.
- The CSA S16 and AISC 360 beam design equations may be used to conservatively predict the moment resistances of I-shaped welded steel girders with web slenderness ratios near the CSA S16 Class 2/3, or AISC compact/noncompact, boundary by setting the St. Venant torsional constant equal to zero.
- The stability response of I-shaped single-overhanging steel girders is governed by two failure modes, including, plastic hinging at the back span or at the fulcrum support, and inelastic LTB at the cantilever segment. The first mode of failure was generally observed in the specimens with high load ratios (e.g., 0.85), whereas low load ratios (e.g., 0.25) and lack of lateral support at the cantilever tip resulted in LTB at the cantilever.
- A regression-based method was proposed to determine the flexural capacity of overhanging steel girders. The proposed method relates the factored moment resistance of an overhanging beam to the plastic moment capacity of the cross-section and a moment modification factor that accounts for the elastic LTB capacity of the girder, the moment gradient within the back span, lateral bracing conditions at the cantilever tip and web slenderness ratio.
- A multi-axis pseudo-dynamic hybrid test was developed for the evaluation of the stability response of steel braced frames with emphasis on the buckling of wide-flange columns. A case study consisting of a full-scale multi-axis pseudo-dynamic hybrid test was performed to examine the seismic stability of two-tiered concentrically braced frames, which confirmed the concerns associated with the stability of their columns and the need for enhanced seismic design method to protect the columns of steel multi-tiered braced frames from yielding and instability.
- Two failure modes dominate the stability response of deep wide-flange columns located at the first story of steel MRFs: 1) out-of-plane buckling at the column base associated with severe local buckling, observed in shorter columns ($L \leq 4.3$ m); 2) member buckling associated with lateral out-of-plane deformation over the column length, recorded for longer columns ($L \geq 5.3$ m). Both failure modes were accompanied by severe strength degradation resulting in flexural strength falling below 50% of the plastic moment capacity of the column.
- An equation that couples the global slenderness, cross-section aspect ratio and axial load ratio was developed to predict the out-of-plane stability condition of wide-flange columns with base plastic hinging in Ductile steel MRFs. This equation offers a more representative and inclusive stability design check than a set of uncoupled lateral bracing and axial force ratio checks currently prescribed by 2019 CSA S16.

– The lessons learned from the challenges associated with designing experimental programs or developing numerical models for stability response evaluation, along with the techniques developed to overcome these challenges, will contribute to future research in structural stability.

Acknowledgments

The research projects presented in this paper were funded by the Natural Sciences and Engineering Research Council (NSERC) of Canada, the University of Alberta Centre for Steel Structures Education and Research (The Steel Centre), and the Canadian Institute of Steel Construction. Steel materials for the welded girder specimens were donated by SSAB and fabrication of the girders and ancillary testing fixtures was completed by Supreme Group. All steel materials for the overhanging beam specimens and ancillary testing fixtures were donated by Supreme Group. Steel materials for the braced frame hybrid test specimens were provided by CANAM. These contributions are gratefully acknowledged. The author would like to acknowledge the contributions of the research collaborators, Prof. Robert Driver from the University of Alberta and Prof. Robert Tremblay from Polytechnique Montreal, and thank graduate research assistants, Abrar Islam, Dimple Ji, Guillaume Toutant, Maha Essa, Pablo Cano, Sheldon Twizell, Vahab Esmaeili and Yasaman Balazadeh Minouei. The author sincerely thanks the technical staff and engineers at the I.F. Morrison Structural Engineering Laboratory of the University of Alberta, Greg Miller and Cameron West, and at the Structural Engineering Laboratory of Polytechnique Montreal, Martin Leclerc and Romain Siguier for their valuable advice and assistance during the test programs. The author expressed his sincere appreciation to Shawn Yu of MTS Systems for his assistance in performing hybrid testing.

References

AASHTO. (2020). *AASHTO LRFD Bridge Design Specifications*. American Association of State Highway and Transportation Officials, Washington, DC.

AISC. (2010a/2016a). ANSI/AISC 341-10/16, *Seismic Provisions for Structural Steel Buildings*. American Institute of Steel Construction, Chicago, IL.

AISC. (2010b). ANSI/AISC 360-10, *Specification for Structural Steel Buildings*. American Institute of Steel Construction, Chicago, IL.

AISC. (2022). *ANSI/AISC 360-22, Specification for Structural Steel Buildings*. American Institute of Steel Construction, Chicago, IL.

ASCE. (2010). SEI/ASCE 7-10, *Minimum Design Loads for Buildings and Other Structures*. American Society of Civil Engineers.

AWS (2015). *Structural Welding Code—Steel*. AWS D1.1/D1.1M:2015. American Welding Society, Miami, FL.

Balazadeh-Minouei, Y., Koboevic, S., Tremblay, R. (2017). "Seismic evaluation of a steel braced frame using NBCC and ASCE 41." *J. Const.r Steel. Res.*, 135: 110–124.

Bjorhovde, J., Brozzetti, J., Alpsten, G.A., Tall, L. 1972. "Residual stresses in thick welded plates." *Welding Journal*, 51(8), 392-405.

Cano, P.A., Imanpour, A. (2020). "Evaluation of AISC Seismic Design Methods for Steel Multi-Tiered Special Concentrically Braced Frames." *Eng. J. AISC*., 57(3): 193-214.

CEN. (2005). *Eurocode 3 – Design of Steel Structures, DD EN-1993-1:2005*. E, Comité Européen de Normalisation, Brussels, Belgium.

Chernenko, D. E., Laurie Kennedy, D. J. 1991. "An analysis of the performance of welded wide flange columns." *Can. J. Civ. Eng.*, 18(4), 537-555.

CISC. (2014). *Moment Connections for Seismic Applications,* 2nd Edition. Canadian Institute of Steel Construction. Markham, ON.

Closkey, Dan J. (1988). "Report of the Commissioner Inquiry Station Square Development." Province of British Columbia, Burnaby, BC.

CSA. 2019a. *CSA S16-19, Design of steel structures*. Canadian Standards Association, Mississauga, ON.

CSA. 2019b. *CSA S6-19, Canadian Highway Bridge Design Code*. Canadian Standards Association, Mississauga, ON.

CSA. (2018). *W59-18 Welded steel construction (metal arc welding)*. Canadian Standards Association, Missisauga, ON.

Elkady, A., and Lignos, D.G. (2015). “Analytical investigation of the cyclic behavior and plastic hinge formation in deep wide-flange steel beam-columns.” *Bull. Earthq. Eng.*, 13(4), 1097–1118.

Elkady, A., Lignos, D. G. (2018a). “Full-scale testing of deep wide-flange steel columns under multi axis cyclic loading: Loading sequence, boundary effects, and lateral stability bracing force demands.” *ASCE, J. Struc. Eng.*, 144(2), 04017189.

Elkady, A., Lignos, D. G. (2018b). Improved seismic design and nonlinear modeling recommendations for wide-flange steel columns. *ASCE, J. Struc. Eng.*, 144(9), 04018162.

Esmaeili, V., Imanpour, A., Driver, R. G. (2021). "Stability of Gerber Systems with Top-flange Bracing." *Annual Stability Conference*, Structural Stability Research Council, Louisville, KY.

Essa, M., Driver, R. G., Imanpour, A. (2024). “Experimental testing of single-overhanging I-shaped steel girders.” *Annual Stability Conference*, Structural Stability Research Council, San Antonio, TX.

Imanpour, A., Tremblay, R., Davaran, A., Stoakes, C., and Fahnestock, L. A. (2016). “Seismic Performance Assessment of Multitiered Steel Concentrically Braced Frames Designed in Accordance with the 2010 AISC Seismic Provisions.” *ASCE, J. Struc. Eng.*, 142(12): 04016135.

Imanpour, A., Tremblay, R., Fahnestock, L.A., Stoakes, C. (2016b). “Analysis and Design of Two-Tiered Steel Braced Frames under In-Plane Seismic Demand.” *ASCE, J. Struc. Eng.*, 142(2).

Imanpour, A., Tremblay, R. (2016). “Seismic design and response of steel multi-tiered concentrically braced frames in Canada.” *Can. J. Civ. Eng.*, 43: 908-919.

Imanpour, A., Tremblay, R., Leclerc, M., Siguier, R. (2018). “Development of Hybrid Simulation Computational Model for Steel Braced Frames.” 9th *International Conference on Behavior of Steel Structures in Seismic Area*, STESSA, Christchurch, New Zealand.

Imanpour, A., Tremblay, R., Leclerc, M., Siguier, R., Guillaume, T., Balazadeh-Minouei, Y., You, S. (2021). “Development and Application of Multi-Axis Hybrid Simulation for Seismic Stability of Steel Braced Frames.” *Engineering Structures*. 252, 113646.

Islam, A., and Imanpour, A. (2022). “Stability of wide-flange columns in steel moment-resisting frames: evaluation of the canadian seismic design requirements.” *Bull. Earthq. Eng.*, 20, 1591–1617.

Islam, A., and Imanpour, A. (2023). “Seismic stability of steel wide-flange columns in ductile moment-resisting frames: out-of-plane response and design recommendations.” *Bull. Earthq. Eng.*, 21, 3493–3519.

Ji, D. Twizell, S. C., Driver, R. G., Imanpour, A. (2022). “Lateral–Torsional Buckling Response of Compact I-shaped Welded Steel Girders”, *ASCE, J. Struc. Eng.*, 148(10), 04022149.

Lacerte, M., Tremblay, R. (2006). “Making use of brace overstrength to improve the seismic response of multistorey split-X concentrically braced steel frames.” *Can. J. Civ. Eng.*, 33(8): 1005–1021.

Lai, J.-W., Mahin, S. A. (2015). “Strongback System: A Way to Reduce Damage Concentration in Steel-Braced Frames.” *ASCE, J. Struc. Eng.*, 141(9): 04014223.

MacRae, G. A., Kimura, Y., and Roeder C. (2004). “Effect of Column Stiffness on Braced Frame Seismic Behavior.” *ASCE, J. Struc. Eng.*, 130:3(381), 381-391.

McKenna, F., M. H. Scott, and G. L. Fenves. (2010). “Nonlinear finite element analysis software architecture using object composition.” *J. Comput. Civ. Eng.*, 24 (1): 95–107.

Metten, A. (2019). “Structural Design of the Gerber Girder Cantilever System – Filling the Knowledge Gap [Conference presentation].” *The Canadian Steel Conference*, Canadian Institute of Steel Construction, Montreal, Quebec.

Newell, J., and Uang, C-M. (2008). “Cyclic behavior of steel wide-flange columns subjected to large drift.” *ASCE, J. Struc. Eng*., 134(8), 1334–1342.

NRC. (2015/2020). *National Building Code of Canada (NBCC)*. Associate Committee on the National Building Code, Ottawa, ON.

Ozkula, G., Harris, J., Uang, C-M. (2017a). “Classifying Cyclic Buckling Modes of Steel Wide-Flange Columns under Cyclic Loading.” *ASCE Structures Congress*, Denver CA, pp. 155-167.

Ozkula, G., Harris, J., Uang, C-M. (2017b). “Observations from Cyclic Tests on Deep Wide-Flange Beam-Columns.” *AISC Eng. Journal*, 1st Quarter, 45–59.

Ozkula, G., Uang, C.-M., Harris, J. (2021). “Development of Enhanced Seismic Compactness Requirements for Webs in Wide-Flange Steel Columns.” *ASCE, J. Struc. Eng.*, 147(7), 04021100.

Phillips, M., Kamath, A.M., Sherman, R.J., White, D.W. (2023). “Influence of web distortion and onset of yield on doubly symmetric built-up I-girders subjected to high moment gradient.” *Thin-Walled Structures*, 185, 110545.

Redwood, R. G., Lu, F., Bouchard, G., Paultre, P. (1991). “Seismic response of concentrically braced steel frames.” *Can. J. Civ. Eng.*, 18(6): 1062–1077.

Simulia Abaqus 6.14.2 (2011). *Abaqus FEA*, www.simulia.com.

Slein, R., Kamath, A.M., Phillips, M., Sherman, R.J., Scott, D.W., White, D.W. (2023). "Experimental and analytical assessment of LTB resistance of built-up steel I-section members." *J. Const.r Steel. Res.*, 204, 107771.

Tremblay, R. (2000). "Influence of brace slenderness on the seismic response of concentrically braced steel frames." *the Third International Conference STESSA 2000*, pp. 527–534

Tremblay, R., Lacerte, M. (2002). "Influence of the properties of bracing members on the seismic response of concentrically braced steel frames." *the 12th European Conference on Earthquake Engineering*, Paper 481.

Tremblay, R. (2003). "Achieving a stable inelastic seismic response for multi-story concentrically braced steel frames." *Eng. J. AISC*., 40(2): 111–129.

Tremblay, R., Poncet, L. (2004). "Improving the seismic stability of concentrically braced steel frames." *Annual Stability Conference, Structural Stability Research Council*, pp. 19–38.

Twizell, S.C., Ji, D., Imanpour, A., Driver, R. G. (2023). "Lateral–Torsional and Distortional Buckling of I-shaped Welded Steel Girders", *ASCE, J. Struc. Eng.*, 149(9), 04023118.

Uang, C.-M., Ozkula, G., Chansuk, P. (2019). "Research on seismic design of deep wide-flange steel columns in the U.S." *12th Pacific Structural Steel Conference*, Tokyo, Japan, Tokyo, Japan.

Unsworth, D., Driver, R. G., Li, L. (2020). "Measurement and prediction of residual stresses in welded girders *J. Const.r Steel. Res.*, 169, 106007.

Uriz, P., Mahin, S. A. (2008). Toward Earthquake-Resistant Design of Concentrically Braced Steel-Frame Structures. Pacific Earthquake Engineering Research Center, *PEER Report 2008/08*.

White, D.W., Jung, S.-K. 2007. "Effect of web distortion on the buckling strength of noncomposite discretely-braced steel I-section members." *Engineering Structures*, 29(8), 1872-1888.

Winter, G. (1943). "Lateral stability of unsymmetrical I-beams and trusses in bending." *Trans. Am. Soc. Civil Eng*. 108 (1): 1851–1864.

Yarimci, E., Yura, J. A., Lu, L. W. (1967). "Techniques for testing structures permitted to sway." *Experimental Mechanics*, 7(8), 321-331.

Ziemian, R. D. (2010). *Guide to Stability Design Criteria for Metal Structures*. 6th Ed., John Wiley & Sons, Inc., Hoboken, NJ.